

Ray-Based Stochastic Inversion

Dennis van der Burg^{*†}, Arie Verdel[°], and Kees Wapenaar^{†, °} Shell EP Technology, [†] Delft University of Technology

Summary

A new seismic inversion method, Ray-Based Stochastic Inversion (RBSI) is presented, which is founded on the high-frequency Asymptotic Ray Theory (ART) description of seismic waves and firmly links Kirchhoff-Helmholtz pre-stack depth migration (PreSDM) with Stochastic Inversion (SI) for reservoir properties. Results from synthetic data tests show that: (1) RBSI, contrary to SI, can correctly determine lateral layer-density variations, a requirement for preserved-amplitude PreSDM, and (2) RBSI can delineate the correct reservoir properties in cases where SI produces erroneous results because of dip-dependent migration stretch.

Ray-Based Stochastic Inversion Principle

For RBSI, the subsurface space $X \subset \mathbb{R}^3$ with surface boundary ∂X is parameterised as an overburden macro-model overlying a layered target reservoir sequence (Fig. 3) and is assumed to satisfy the standard ray-theoretical validity conditions (Červený et al., 1977). Elements \vec{x} of X can be written as (x_1, x_2, x_3) with $x_3 > 0$ and ∂X as $x_3 = 0$. Instead of the 1D convolutional model of SI, in RBSI 3D elastodynamic ray-tracing is used (Fig. 1). In principle, any wave type and acquisition configuration can be handled by RBSI. In this paper, we limit ourselves to surface-recorded single P-reflections. The key vehicle for RBSI is then formed by a single pair of P-rays leaving the specular reflection point $\vec{x}_R \in \Sigma_n$, the n -th reflection surface, within the reservoir sequence at angles θ_n^\pm to the normal-vector $\hat{n}(\vec{x}_R)$ of Σ_n in \vec{x}_R , see Fig. 3. Layer parameters on the lower side of Σ_n are iteratively updated using a Metropolis algorithm (Leguijt, 2001) whereby the mismatch between the modeled $\tilde{u}(\vec{x}_s, \vec{x}_r, \vec{x}_R; t)$ and real $\bar{s}(\vec{x}_s, \vec{x}_r, \vec{x}_R; t)$ reflection is minimised: $\tilde{u}(\vec{x}_s, \vec{x}_r, \vec{x}_R; t)$ is uniquely defined by the single source-receiver pair (\vec{x}_s, \vec{x}_r) , by initial directions (θ_n^\pm, ϕ) (measured from $\hat{n}(\vec{x}_R)$ in the plane of propagation at angle ϕ with the azimuth), by the migration velocity model $v_p(\vec{x})$ and by the source wavelet $\mathcal{F}_0(t)$. Details of the data flow are shown in Fig. 2. Ray-theory requires at least C_2 -smoothness of Σ_n , which has to be determined from reflection event picks on the migrated image. Furthermore, either two-point ray-tracing or interpolations are generally required, to find those values of θ and ϕ that lead to ray-emergence locations \vec{x}_s and \vec{x}_r .

Theory

The asymptotic displacement field vector \vec{u} measured at \vec{x}_r due to a wave emitted at \vec{x}_s and reflected at \vec{x}_R , can be expressed as, see Červený et al. (1977):

$$\vec{u}(\vec{x}_s, \vec{x}_r, \vec{x}_R; t) = \text{Re} \left[\vec{u}^{(0)}(\vec{x}_s, \vec{x}_r, \vec{x}_R) F_0(t - \tau(\vec{x}_s, \vec{x}_r, \vec{x}_R)) \right] \quad (1)$$

where only the leading term (denoted by the zeros in equation

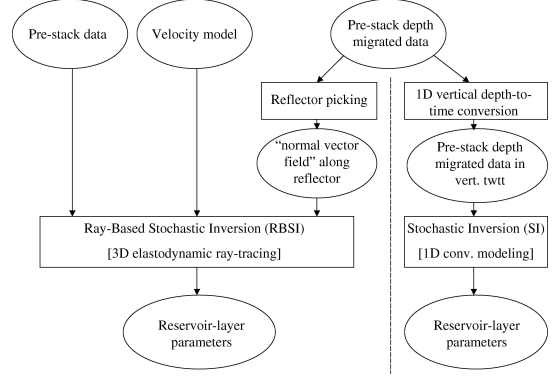


Fig. 1: Flowsheet RBSI and SI for inversion of layer-parameters.

above) of the formal asymptotic ray series expansion solution of the general elastodynamic equation has been used. The isotropic point source is represented by $S(\vec{x}, t) = \mathcal{F}_0(t) A_0(\vec{x}_s) \delta(\vec{x} - \vec{x}_s)$, with A_0 the source strength. Already in slightly more complex media than those presented in this paper, it will be needed to allow handling of phase shifts due to passage of rays through caustics. In that case $\text{Im}[\vec{u}^{(0)}]$ will become nonzero, so that the bandlimited source signal function (source wavelet \mathcal{F}_0) has to be extended to the analytical wavelet $F_0(t) = \mathcal{F}_0(t) + i\mathcal{G}_0(t)$ with \mathcal{G}_0 the Hilbert transform of \mathcal{F}_0 (if caustics are absent: $\mathcal{G}_0=0$). The phase function or eikonal τ is real-valued.

For a model consisting of a 2.5D isotropic-elastic subsurface with constant wave-propagation velocities and layers with C_1 -smooth density gradients (Fig. 3), the x_3 -component of the primary P-wave reflection response of the n -th contrast Σ_n can be calculated analytically using the ART-expression:

$$u_3^{(0)}(\vec{x}_s, \vec{x}_r, \vec{x}_R) = A_0(\vec{x}_s) R^+(\vec{x}_R, \theta_n^+) T(\vec{x}_R, \theta_n^+) D(\vec{x}_R, \theta_n^+) \times C_0(\vec{x}_s, \vec{x}_r, \vec{x}_R) C_1(\vec{x}_s, \vec{x}_r, \vec{x}_R) (l(\vec{x}_s, \vec{x}_R) + l(\vec{x}_R, \vec{x}_r))^{-1} \quad (2)$$

with l the ray path lengths, C_0 the free surface correction factor (Aki and Richards, 1980), C_1 the reflector curvature correction factor, R^+ the Zoeppritz reflection coefficient, and $T = \prod_{i=1}^{n-1} T_i^-(\theta_i^-) T_i^+(\theta_i^+)$ the product of transmission losses of the ray-pair (while crossing $n-1$ contrasts in the overlying overburden plus reservoir); factor D takes into account the amplitude-effects on the rays related to their traversal through density gradients within the n layers overlying Σ_n :

$$D(\vec{x}_R, \theta_n^+) = \prod_{i=1}^n \left(\sqrt{\frac{\rho_i(\vec{x}_{T,i}^+)}{\rho_i(\vec{x}_{T,i}^-)}} \cdot \sqrt{\frac{\rho_i(\vec{x}_{T,i}^-)}{\rho_i(\vec{x}_{T,i-1}^-)}} \right) \quad (3)$$

with $\vec{x}_{T,0}^+ = \vec{x}_s$, $\vec{x}_{T,0}^- = \vec{x}_r$ and $\vec{x}_{T,n}^+ = \vec{x}_{T,n}^- = \vec{x}_R$, see Fig. 3. With our choice of model (Fig. 4), while using normal-incidence

Ray-Based Stochastic Inversion

($\theta_n^+ \equiv 0$)-reflections only, $D = 1$ and the particle velocity data set $\dot{u}_3(\vec{x}_s = \vec{x}_r; t)$ is caustic-free. The expressions for C_1 and R^+ in Eq. 2 then simplify to:

$$R^+(\vec{x}_R, \theta_n^+ = 0) = \frac{\rho_{n+1}(\vec{x}_R) - \rho_n(\vec{x}_R)}{\rho_{n+1}(\vec{x}_R) + \rho_n(\vec{x}_R)} \quad (4)$$

$$C_1(\vec{x}_s = \vec{x}_r, \vec{x}_R) = \sqrt{\frac{r_c^+(\vec{x}_R)}{r_c^+(\vec{x}_R) + l(\vec{x}_s = \vec{x}_r, \vec{x}_R)}} \quad (5)$$

In equation 5, r_c^+ is the reflector radius of curvature at \vec{x}_R , measured from the ray-incidence direction; see Červený et al. (1977, pp. 82–84).

Preserved amplitude PreSDM of the zero-offset particle velocity data set \dot{u}_3 reads (“ $\langle \cdot \rangle$ ” denotes that R^+ is spatially bandlimited):

$$\langle R^+(\vec{x}, \theta_n^+ = 0) \rangle = -\frac{2}{\pi v_0 T(\vec{x}, \theta_n^+ = 0)} \times \int_{-\infty}^{\infty} \int_{-\infty}^{\infty} \frac{\partial}{\partial t} \dot{u}_3(\vec{x}_s = \vec{x}_r; t)|_{t=t_d} dx_{1r} dx_{2r} \quad (6)$$

in which t_d represents the two-way time between \vec{x} and $\vec{x}_s = \vec{x}_r$, and $v_0 = v_p$.

Numerical Examples

Lateral Layer-Density Variations

To establish the potential of RBSI for determining laterally variable layer-properties, a series of synthetic data tests was performed using the simple model presented in Fig. 4: a 2.5D isotropic-elastic subsurface with constant background density of 2000 kg/m^3 , constant wave propagation velocities (resulting in straight rays) $v_p=2500 \text{ m/s}$ and $v_s=v_p/1.7$, and containing three layers with densities that differ from the background. The three contrasting layers are bounded by Gaussian reflectors Σ_i that are C_2 -smooth and contain, also Gaussian, layer-density variations ρ_k :

$$\Sigma_i(x_1) = z_{max,i} - \Delta z_i \exp\left(-\frac{(x_1 - \mu)^2}{2\sigma^2}\right) \quad \forall i \in \{1, 2, \dots, 6\} \quad (7)$$

$$\rho_k(x_1) = \rho_{max} - \Delta \rho \exp\left(-\frac{(x_1 - \mu)^2}{2\sigma^2}\right) \quad \forall k \in \{2, 4, 6\} \quad (8)$$

In Eqs. 7 and 8, $\sigma = 1000 \text{ m}$, $\mu = 3000 \text{ m}$, $\Delta z_i = z_{max,i} - z_{min,i}$, where $z_{max,i}$ and $z_{min,i}$ can be read from Fig. 4, and $\Delta \rho = (\rho_{max} - \rho_{min}) = (3000 - 2100) \text{ kg/m}^3$. The model has been carefully chosen to obey all standard ART-validity conditions: it is assumed for our numerical tests that interbed multiples were removed from the pre-stack unmigrated data, that serves as input for the RBSI inversion. The underlying argument for this choice is that we could model (and thus remove) with ART any zero-offset interbed multiple event in the model described above.

In our comparative SI- and RBSI-tests, we computed the zero-offset particle velocity data set $\dot{u}_3(\vec{x}_s = \vec{x}_r; t)$ for 601 source/receiver-positions at 10 m spacing at ∂X using a

Hanning-tapered zero-phase bandpass wavelet with corner frequencies 4-12-50-75 Hz. With this choice of model- and acquisition parameters, \dot{u}_3 is caustic-free and only contains normal-incidence ($\theta_n^+ \equiv 0$)-reflections. Hence, the amplitudes of this data set are described by Eqs. 2 - 5, where we chose $A_0(\vec{x}_s) = 1 \forall \vec{x}_s$. Fig. 5 shows every 20th trace of \dot{u}_3 .

In Fig. 6 the data is shown after “preserved-amplitude” PreSDM (Eq. 6) while using a laterally *constant* density model ($\rho_k = 2100 \text{ kg/m}^3$) such as derived from the density log. A reasonable assumption, as, prior to inversion, we only have density information at the well location (see Fig. 4). We denote “preserved-amplitude” between quotes here, because the migration-image contains incorrect reflection strengths due to usage of the wrong density model. Consequently any subsequent inversion for target reservoir layer densities, and related parameters as porosities and pore fluid saturations, applied on that image, is bound to fail.

Fig. 7 shows the difference between Fig. 6 and the migrated result using the correct, laterally variable, density model (Eq. 8) such as can be obtained from the pre-stack data using RBSI (see Fig. 2). This difference becomes larger further away from the well location because of the increasing difference between assumed and actual layer-densities, and deeper down in the model because of the accumulating errors due to incorrect transmissions. This is also expressed in Fig. 8 which shows the reflection amplitude along Σ_6 after preserved-amplitude PreSDM using both a laterally constant density model (black line) and the exact density model (grey line), in comparison with the theoretical reflection coefficient (dashed line), which is the ideal preserved-amplitude PreSDM result.

In Fig. 9, inversion results are shown for ρ_6 : SI (lower curve) versus RBSI; error bars denote standard deviations. The reflection strengths as determined from RBSI are almost identical to those described by theory (Eq. 4), whereas the SI-results, including their error bars, map outside the desired results.

Strongly Dipping Subsurface Structures

In order to systematically investigate the detrimental effect of dip-dependent migration-induced wavelet stretch (Levin, 1998) on SI, the three contrasting layers of the previous example were replaced by a single wedge-like density contrast (see inset Fig. 10). Although this model is not strictly obeying all ART-validity conditions, the zero-offset inter-bed multiples can again be accurately modeled with ART, and hence removed from the data prior to inversion. Fig. 10 shows a detail of two ideal migration results: one that includes the effect of wavelet stretch (varwig display) and one without (wiggle display). Only the latter, fictitious, case fulfills the wavelet requirements for SI.

The barplots in Fig. 11 represent the inversion results for SI and for RBSI respectively (the latter was run on the normal-incidence data that are not shown here). It can be seen that RBSI determines the density of the middle layer much better than SI.

Outlook

The encouraging results of first, orientating, synthetic data tests indicate that investigation of more realistic models is opportune: RBSI’s robustness should be tested in the presence of complex velocity models, velocity uncertainties, wavelet errors and noise

Ray-Based Stochastic Inversion

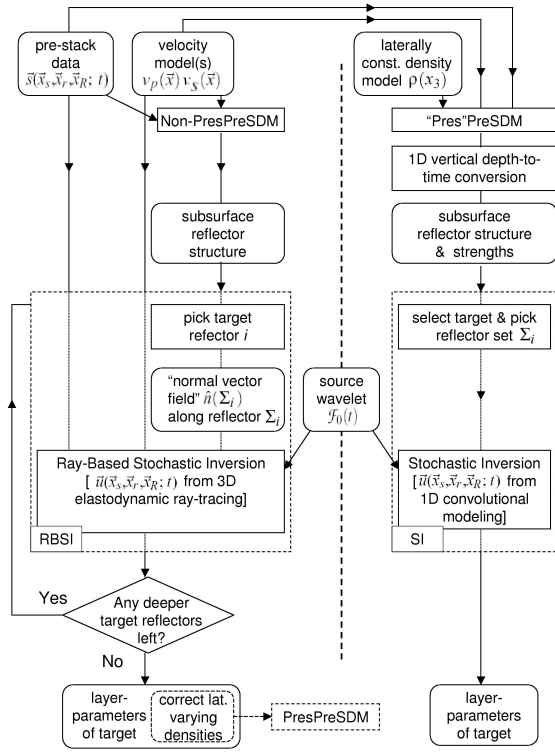


Fig. 2: Detailed flowsheet RBSI and SI for inversion of layer-parameters (Pres is short for preserved-amplitude). The 3D initial, laterally constant, density model is determined from well-data; the 3D velocity models are determined by velocity analysis, constrained by well-data.

in general. Also, extension to finite offset configurations will be investigated.

Acknowledgment

The authors wish to thank Shell EP Technology for financially supporting the research project and permission to publish this work.

References

- Aki, K., and Richards, P., 1980, Quantitative seismology: Freeman, Books in Geology, 1, 190.
- Červený, V., Molotkov, I., and Pšenčík, I., 1977, Ray method in seismology: Univerzita Karlova, Praha.
- Leguijt, J., Jun 2001, A promising approach to subsurface information integration: EAGE Extended Abstracts, pages L–35.
- Levin, S., Mar 1998, Resolution in seismic imaging: Is it all a matter of perspective?: Geophysics, 63, no. 2, 743–749.

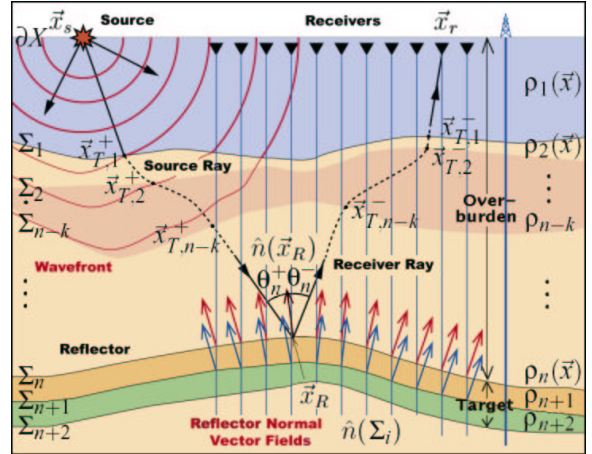


Fig. 3: Subsurface Parameterisation for RBSI.

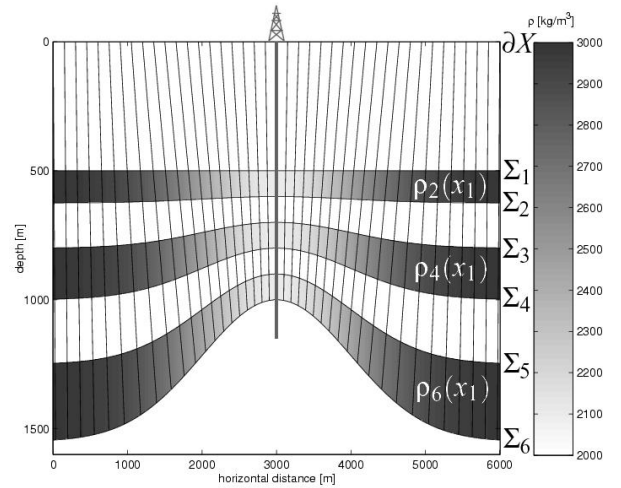


Fig. 4: Zero-offset rays in Gaussian density model.

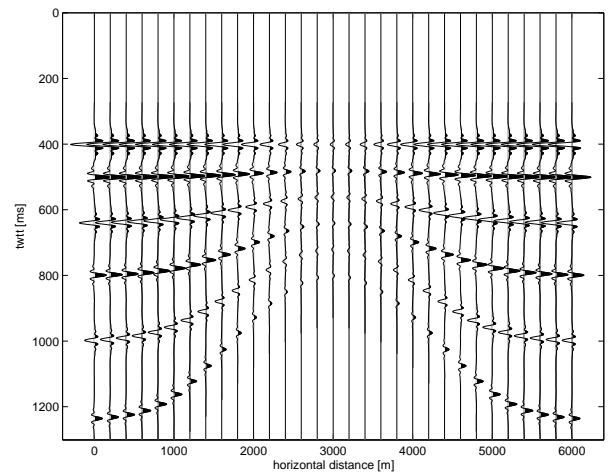


Fig. 5: Dataset u_3 corresponding to Fig. 4.

Ray-Based Stochastic Inversion

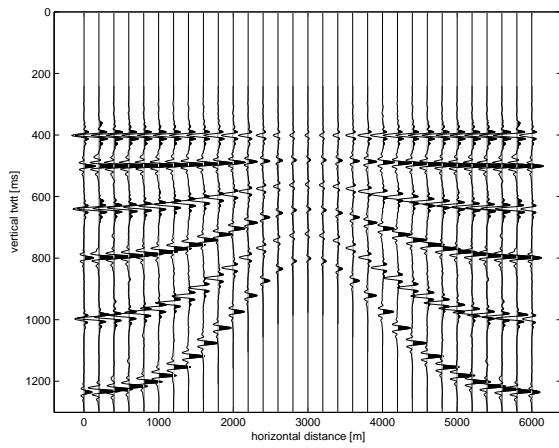


Fig. 6: Preserved-amplitude zero-offset depth migration with laterally constant density model from well.

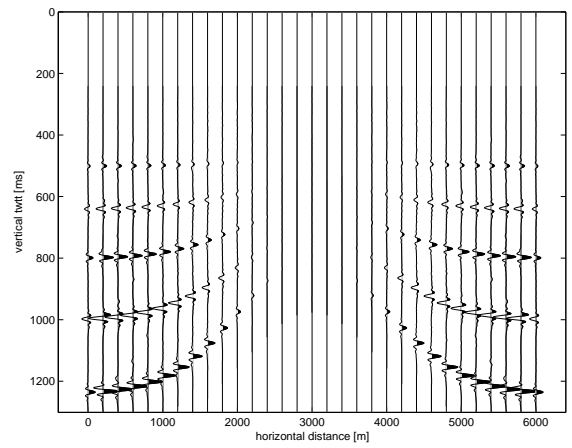


Fig. 7: Difference between Fig. 6 and migration using exact density model from RBSI.

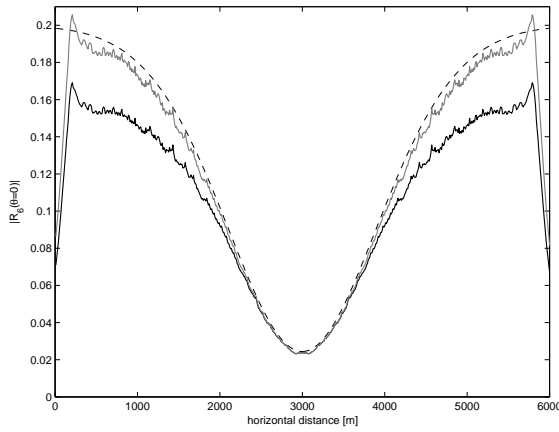


Fig. 8: Reflection-amplitude along Σ_6 after migration using constant-density layers (black line) and exact density model (grey) as compared to $R^+(\bar{x}_R, \theta_6^+ = 0)$ (dashed).

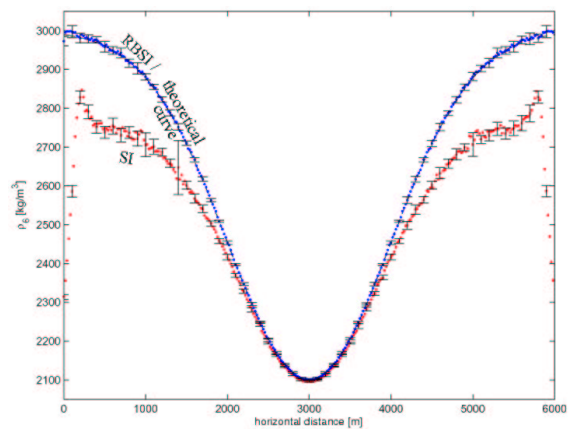


Fig. 9: ρ_6 from SI and RBSI, the latter converging to desired value. Error bars denote standard deviations.

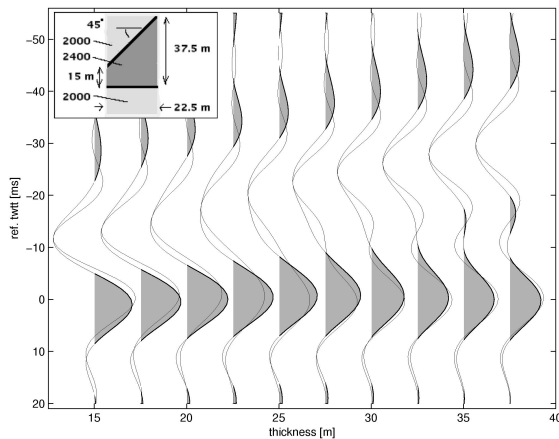


Fig. 10: Detail of ideal migration result of wedge model.

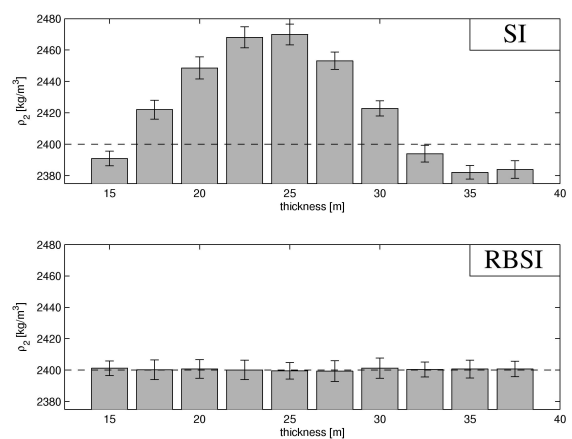


Fig. 11: Density of middle layer of wedge model (inset Fig. 10) as determined from SI (top) and RBSI (bottom). Dashed line: desired result.